MATERIALS CHEMISTRY FRONTIERS

ARTICLE

Received 00th January 20xx,
Accepted 00th January 20xx

DOI: 10.1039/x0xx00000x

www.rsc.org/

Stable Luminous Nanocomposite of $CsPbX_3$ Perovskite Nanocrystal Anchored on Silica for Multicolor Anti-counterfeit Ink and White-LED

Aizhao Pan,*[a] Yanan Li,[a] Youshen Wu,[a] Ke Yan,[b] Matthew Jurow,[c] Yi Liu,*[c] Ling He*[a]

Inorganic perovskite ($CsPbX_3$, X=Cl, Br and I) nanocrystals (NCs) have received great attention for their fascinating optoelectronic properties. However, their potential applications are primarily limited by the instability arising from their mobile ionic nature. Herein, we introduce a facile and effective templated synthetic strategy to prepare extremely stable $CsPbX_3$ nanocomposites, denoted as $CsPbX_3$@CA-SiO_2, by *in-situ* anchoring of $CsPbX_3$ NCs onto octadecyl/propylamine capped silica particles (SiO_2 NPs). The two-step synthesis involves first the preparation of amino-group capped silica NPs from a mixed 3-aminopropyltriethoxysilane (APTES) and trimethoxy(octadecyl)silane (TMODS) precursor, which were utilized to induce nucleation and growth of $CsPbX_3$ nanocrystals to give $CsPbX_3$@CA-SiO_2 composites with monodispersed $CsPbX_3$ NCs (~6 nm). The emission wavelength of the resulting composite can be tuned between 400 and 650 nm by controlling the halide composition while maintaining a high photoluminescence quantum yield (PLQY=76%). The as-fabricated composites exhibit remarkable photostability and water stability, both uncommon in these materials. The $CsPbX_3$@CA-SiO_2 composite can also be used to create an anti-counterfeit ink and down-converting white light emitting diode (WLED). This work provides a valuable approach for the production of future optoelectronic devices, catalysts and sensors based on perovskite NCs.

Introduction

Recently, inorganic lead halide-based perovskite nanocrystals $CsPbX_3$ NCs (X = Cl, Br or I) have drawn broad attention from groups around the world because of their exceptional optoelectronic characteristics, such as high quantum yields (QYs □ 90%), narrow emission lines, controllable bandgaps and high carrier mobility.[1-5] These prominent optoelectronic properties make them promising candidates for light-emitting diodes (LED), lasers, solar cells, photodetectors and display backlights.[5-8]

Despite their outstanding optoelectronic properties, large-scale and practical applications are seriously limited by the materials' inherent defects and instability[9-10] towards polar solvents and environmental humidity.[1, 11] In addition, exposure to heat, halides or intense light also produce energy shifting, luminescent peak broadening, severe PL quenching and unacceptably short device lifetimes.[12-15]

To overcome the inherent vulnerability, many strategies have been adopted to stabilize $CsPbX_3$ including: regulating surface ligands (the inclusion of long-chain, branched or sterically hindered surfactant as capping ligands),[16-20] modifying crystal composition (Mn doping),[21-22] incorporating NCs into a protective inorganic matrix (SiO_2, MOF or zeolite-Y) [23-26] or polymers (polystyrene, polymethyl methacrylate, polyvinylidene fluoride, block copolymer micelles or POSS-based polymers)[27-30] etc. These treatments can dramatically enhance the NC's stability by providing a physical barrier. However, most of these approaches were either only suitable for the preparation of luminescent films or bulk materials, were not water resistant, or were not UV stable. The realization of a scalable and stable perovskite nanocomposites remains a challenge.

[a] *Department of Chemistry, School of Science, Xi'an Jiaotong University, Xianning West Road, 28, Xi'an, 710049, China. Email: panaizhao2017032@xjtu.edu.cn, heling@mail.xjtu.edu.cn.*
[b] *Key Laboratory of Education Ministry for Modern Design and Rotor-Bearing System, Xi'an Jiaotong University, Xi'an 710049, China,*
[c] *The Molecular Foundry and Materials Sciences Division, Lawrence Berkeley National Laboratory, Berkeley, California 94720, United States.*
Electronic Supplementary Information (ESI) available. See DOI: 10.1039/x0xx00000x

To generate a stable perovskite light emitter, it is essential to explore a facile and efficient method to produce monodispersed and stable NC-based composites. Silica is an ideal candidate for protecting NCs because of its excellent stability, easy surface functionalization, large surface area, nontoxic earth abundance, and ability to isolate individual NPs to prevent sintering.[24-25, 31] In this study, we apply an *in-situ* templated growth method to anchor the $CsPbBr_3$ NCs on amino-ligand functionalized SiO_2 particles. The capped silica particles were prepared by anisotropic deposition of the hydrolyzed APTES and TMODS with *pre*-obtained SiO_2 particles. The alkylamine chains on SiO_2 particles then serve as surface ligands, preferentially coordinating the perovskite precursors (Pb^{2+} or Cs^+) to form nucleation points and templating the formation of homogeneous NCs composites.[29, 32] The perovskite NCs can be separated from each other and permanently anchored onto the surface of silica spheres to create a very stable material.[31] The photostability and the stability towards water of the resulting $CsPbBr_3$@CA-SiO_2 composites were evaluated by tracking the material's relative PLQY over time of exposure. As a proof of concept, we then applied these composites as an ink for counterfeit-proof signs and as a green fluorophore in a white light emitting diode (WLED) device.

Experimental

Materials and Chemicals:

$PbBr_2$ (99.90%), $PbCl_2$ (99.90%) PbI_2 (99.90%), Cs_2CO_3 (99.99%), octadecene (ODE, 90%), oleic acid (OA, 90%, AR), oleylamine (OLA, 90%, AR), trimethoxy(octadecyl)silane (TMODS, 90%), 3-aminopropyltriethoxysilane (APTES, 99%), vinyltrimethoxysilane (VTMS, 98%), thioglycolic acid (TA, 90%, AR) and tetraethoxysilane (TEOS, >98%) were purchased from Aladdin and used as received without purification. Silicone resin and phosphor fluorescent powder (red) were purchased from Shenzhen Looking Long Technology co., LTD and used as received without purification. All the other solvents were used as received without any purification.

Preparation of silica (SiO_2) NPs:

SiO_2 NPs were synthesized via the modified Stöber method:[33] a solution of TEOS (8 ml), EtOH (150 ml), ammonium hydroxide (12 ml) and deionized H_2O (30 ml) was introduced into a 250 ml round-bottom glass flask and mixed homogenously with a magnetic stirrer. The hydrolysis and condensation reaction of TEOS was carried out under continuous magnetic stirring at a rate of 700 r/min at 50 ℃, from which SiO_2 NPs were obtained as a suspension after 24 h.

Preparation of octadecyl/propylamine-capped silica (CA-SiO_2) NPs:

Octadecyl/propylamine-capped silica NPs were synthesized using the following procedures (Supporting information, Scheme S1). When the above SiO_2 NPs suspension was cooled to room temperature, a mixture of APTES (4 ml) and TMODS (4 ml) was injected gradually. After the magnetic stirring was continued for another 24 h, the white capped SiO_2 NPs (CA-SiO_2) powder was obtained by removing the residual reactant and ammonium hydroxide through five cycles of centrifugation/redispersion in ethanol and water, and finally drying in a vacuum oven at 50 ℃ for 24 h. Similarly, propylamine-capped silica (A-SiO_2) NPs and octadecyl/carboxyl-capped silica (CC-SiO_2) NPs were synthesized using the procedures outlined in Scheme S2.

***In-situ* growth of $CsPbX_3$ NCs on capped CA-SiO_2 NPs ($CsPbX_3$@CA-SiO_2):**

$CsPbX_3$@CA-SiO_2 composites were prepared following a modified procedure.[31] A typical synthetic procedure is described in Scheme 1. Cs_2CO_3 (0.1 mmol), $PbBr_2$ (0.2 mmol) or equivalent PbI_2, $PbBr_2$/$PbCl_2$ and $PbCl_2$, CA-SiO_2 NPs (0.3 g), ODE (10 mL), OLA (0.3 mL), and OA (1 mL) were mixed and heated under vigorous stirring at 150 ℃. The reaction was cooled in an ice/water bath in 5 min. The centrifugation/redispersion procedure was repeated three to five times in toluene, after which the solid precipitate was collected for characterization. The resulting composite was dried in a vacuum oven overnight before being stored for future use. A control sample was made from physically blended silica NPs with $CsPbBr_3$ NCs.

Stability Tests:

To evaluate the stability in water, all composite films were immersed in air-free de-ionized water stored in the dark at room temperature and PL intensity was subsequently measured over time. Separately, colloidal suspensions of $CsPbX_3$@CA-SiO_2 were stored under vacuum at room temperature and subjected to UV light irradiation (365 nm, 0.5 $W{\cdot}cm^{-2}$) over different period of times. The aged samples were then subjected to further characterization.

Anti-counterfeiting inks for patterning:

The composites were dispersed in toluene at a concentration of 0.2 $g{\cdot}mL^{-1}$. Pre-designed seals with "XJTU" patterns were wetted with the above suspension and then pressed against filter papers to transfer the designed patterns.

White LED device fabrication:

To fabricate white LEDs, a blue (460 nm) LED chip was used to excite the green (520 nm for $CsPbX_3$@CA-SiO_2) and red composites (660 nm, YAG fluorescent powder). Firstly, the YAG phosphors (0.3 g) were dispersed in silicon resin (3 g) after vigorous stirring, and the resulting mixture was directly coated onto blue LED chips and thermally cured at 40 ℃ for 30 min and then 120 ℃ for 60 min. Then, the composites film was prepared similarly as above, which would be stowage onto the upper surface of YAG-based LED devices by mixing with silicon resin, followed by two-stage thermal curing, to give the fabricated WLED devices.

Characterization Methods:

Ultraviolet and visible absorption (UV-vis) spectra of colloidal solutions were collected using a Cary 5000 UV-Vis-NIR spectrophotometer. Fluorescence spectra and absolute photo-luminescent quantum yields (PLQYs) were collected using an integrated sphere, recorded on an Edinburgh Instruments

FLS920 spectrophotometer. FTIR spectrometer for the chemical structures were collected using a Tensor 27 of Bruker Optics. PXRD data were acquired using a Bruker AXS D8 Discover X-Ray Diffractometer at a wavelength of Cu K (1.79 Å). X-Ray photoelectron spectroscopy (XPS) measurement for elemental composition was processed about the composites powder by an AXIS ULTRA (England, KRATOS ANALYTICAL Ltd) using an Al mono Kα X-ray source (1486.6 eV) operated at 150 W. SEM images were acquired on a JEOL 7800F Field Emission Scanning Electron Microscope. TEM and high-resolution TEM (HR-TEM) data were acquired on a FEI G_2F_{30} electron microscope operated at 200 kV with a Gatan SC 200 CCD camera.

Results and Discussion

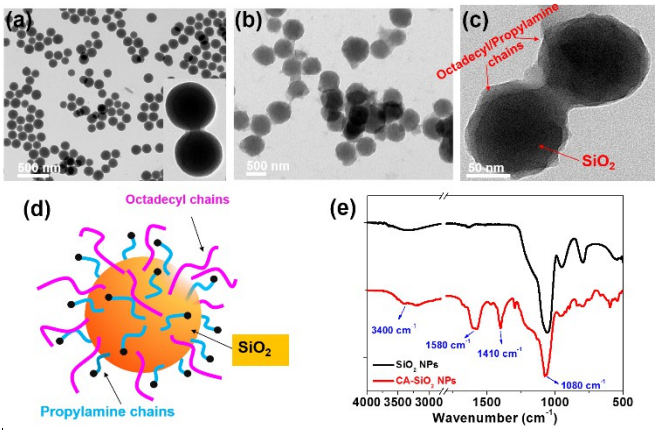

Figure 1. Morphologies and structures of octadecyl/propylamine capped silica (CA-SiO_2) NPs. TEM images of pristine silica (a), octadecyl/propylamine capped silica NPs (b and c). (d) The schematic image of the capped silica NPs. (e) FTIR spectra of the capped (bottom) and pristine (top) silica.

We used octadecyl/propylamine capped silica spheres (SiO_2 NPs) as a substrate for the growth of $CsPbBr_3$ NCs. Firstly, the engineered SiO_2 NPs were synthesized by hydrolysis and condensation of *pre*-obtained SiO_2 NPs with APTES and TMODS. The capped silica (CA-SiO_2) NPs were characterized by transmission electron microscopy (TEM, Figure 1). The functionalized silica particles present a uniform spherical morphology with a silica core and an octadecyl/propylamine shell. The particle diameter is approximately 115 nm, slightly larger than the primal silica particles (ca. 110 nm).

Functionalized silica particles were further characterized by Fourier transform infrared (FTIR) spectra and X-ray photoelectron spectroscopy (XPS). FTIR spectroscopy present strong band at 1100 cm^{-1} and 800 cm^{-1}, assigned to the asymmetric stretching vibration, and symmetric stretching and deformation vibration of Si-O-Si (Figure 1e). Several new peaks appear in the spectra of the functionalized silica, such as the vibrations of symmetric and asymmetric stretching vibrations of $-CH_2-$ and $-CH_3$ (2850 cm^{-1} and 2925 cm^{-1}), asymmetric deformation vibration of $-CH_3$ (1410 cm^{-1}) and specific deformation vibration of NH_2 (1560 cm^{-1}). XPS studies confirm the chemical element composition of CA-SiO_2 NPs (Figure S1a) by the emerging peak at 401.88 eV for the binding energy of N1s. Thermogravimetric analysis yields a quantitative organic content about 16 wt% of CA-SiO_2, close to the amount of silane (APTES and TMODS) added (Figure S1b). Therefore, a core-shell structural schematic drawing of the CA-SiO_2 NPs is depicted in Figure 1d, featuring the silica core capped with octadecyl and propylamine groups.

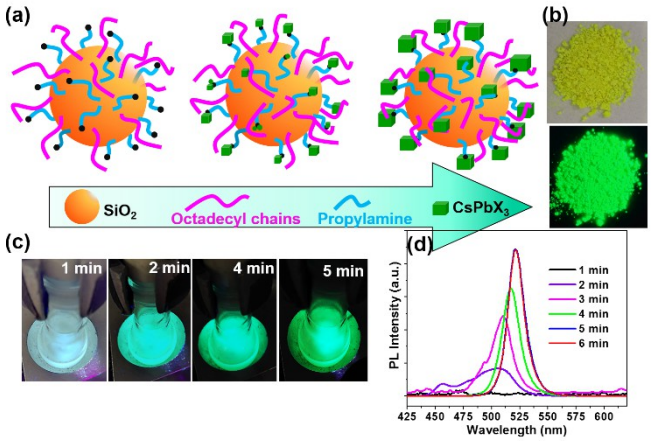

Figure 2. (a) Schematic illustration of the synthesis of $CsPbBr_3$@CA-SiO_2. (b) Digital images of the composites under daylight and UV light. (c) Digital images of the reaction as a function of reaction time (0-5 min). (d) Photoluminescence spectra of the $CsPbBr_3$@CA-SiO_2 composites as a function of reaction time.

Generally, amino or carboxyl end groups coordinate precursors (Pb^{2+} and Cs^+) to form nucleation points at which the PNCs grow.[29, 32] Herein, an *in-situ* growing mechanism for fabricating nanocomposite by anchoring $CsPbX_3$ spatially on SiO_2 particles is proposed in Figure 2a. During the initial reaction system, nucleation can take place on the capped silica NPs' surface. Then, the precursors will further attach on the capped silica spheres surface over time, yielding $CsPbBr_3$@CA-SiO_2 composites with high luminescence.

As the reaction progresses, the transparent solution changes to glaucous and purple-blue emission under UV light, subsequently to blue and green (Figure 2c). To gain insight into the reaction process, *in-situ* PL spectra as a function of reaction time were measured with an interval of 1 min in Figure 2d. Initially no emission was detected. After 2 min, a weak and broad blue emission at 460-520 nm was observed, deriving from the nucleation and preliminary growth of NCs. After 3 and 5 min, cyan and bright green emission can be observed (Figure 2d). With the prolongation of reaction time to 5 min, the PL spectra exhibited a continuous redshift and the PL intensity increased gradually. PL studies indicated that the *in-situ* growth can be quenched within 5 min by ice bath. The dried powder of $CsPbBr_3$@CA-SiO_2 also exhibits strong luminescence under UV light, which can be used as high performance solid-state emitters (Figure 2b).

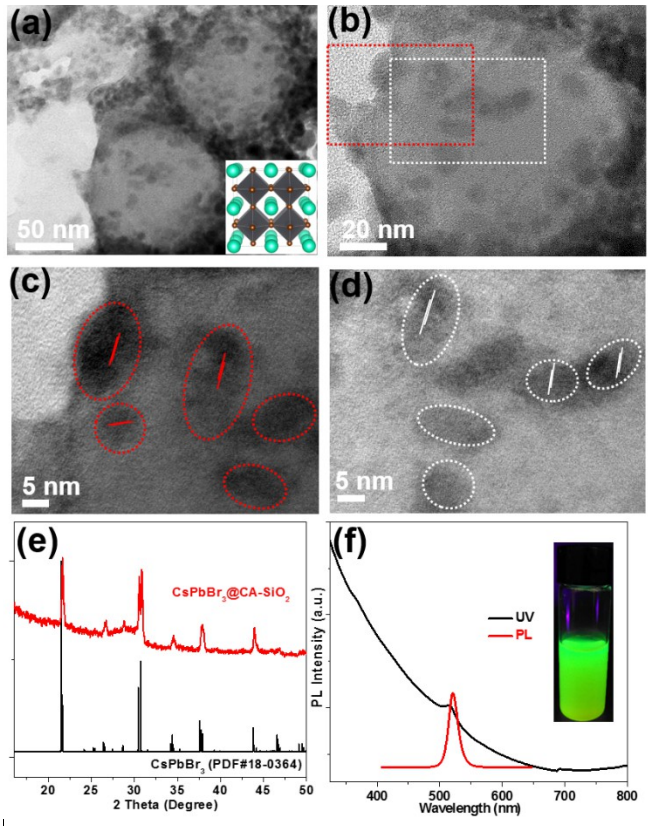

Figure 3. Morphologies, chemical structures and optical properties of the $CsPbBr_3$@CA-SiO_2 composite. TEM (a), high-magnification TEM (b and d) and high resolution TEM (HR-TEM) images (c and e). The inset in (a) is a schematic image of the crystal structure of $CsPbBr_3$. (e) XRD pattern with the standard orthorhombic crystal structure of $CsPbBr_3$. (f) Optical absorption and PL emission spectra. Inset in (f) is a photograph of the colloidal solution of the composites under UV light.

TEM show spherical shaped composites with fairly uniformly distributed NCs adhering on the surface of silica sphere (Figure 3a and b). No obvious large particles are observed. High resolution TEM (HR-TEM) shows the crystallinity of $CsPbBr_3$ NCs and an average size of 6 nm (Figure 3c-e). The decorative perovskite NCs surrounded with compact organic layers are notoriously sensitive to electron beam damage, so the HR-TEM images were taken quickly in order to minimize the exposure time.[15, 29] In comparison, SEM images of the blend of silica NPs and pre-obtained perovskite particles (to serve as a control) exhibit obvious phase separation with randomly distributed CA-SiO_2 NPs and $CsPbBr_3$ NCs (Figure S4).

Chemical structure of $CsPbBr_3$@CA-SiO_2 composites was analyzed with XRD, XPS and energy dispersive spectrometer (SEM-EDS) analysis. Powder X-ray diffraction pattern of the $CsPbBr_3$@CA-SiO_2 yielded peaks at 2θ=17.6, 25.1, 35.6, 39.6, 43.5, 50.2, 53.2 and 56.2° in the diffractogram, corresponding well to the orthorhombic $CsPbBr_3$ crystal phase (JCPDF #01-072-7929) (Figure 3f). XPS analyses (Figure S5a) further indicate that the elemental composition of the $CsPbBr_3$@CA-SiO_2 powder contains all the elements expected from the $CsPbBr_3$ NCs (Cs, Br and Pb) and capped SiO_2 (Si, C, N and O). The elemental ratio of Cs:Pb:Br measured by XPS is about 1:1.1:3.2, matching well with the expected ratio of $CsPbBr_3$. SEM-EDS image further confirm the presence of Si, Cs, Pb and Br in the $CsPbBr_3$@CA-SiO_2 composite (Figure S5b).

The UV-Vis absorption and photoluminescence (PL) spectra of the $CsPbBr_3$@CA-SiO_2 composite were shown in Figure 3g. It was found that the $CsPbBr_3$@CA-SiO_2 composite exhibited an absorption onset and PL emission peak at 518 nm and 520 nm, respectively (Figure 3g), with a PLQY value of around 76%, higher than that of previously reported encapsulated NCs.[34-36]

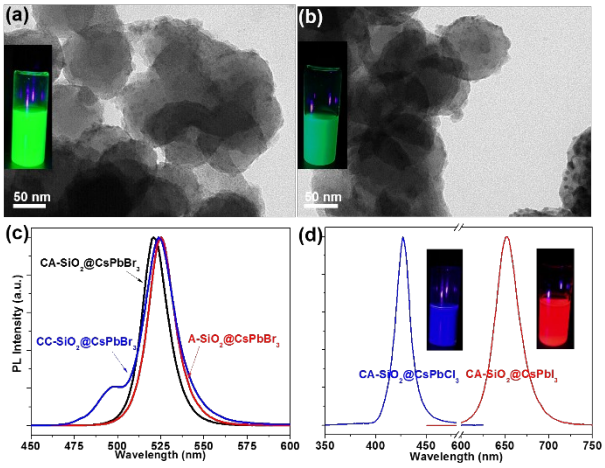

Figure 4. Morphology and optical properties of $CsPbBr_3$@A-SiO_2 and $CsPbBr_3$@CC-SiO_2 spheres. TEM images of the typical $CsPbBr_3$@A-SiO_2 (a) and $CsPbBr_3$@CC-SiO_2 (b). Insets in a) and b) are photographs of the corresponding colloidal solutions under UV light. PL emission spectra of $CsPbBr_3$@CA-SiO_2, $CsPbBr_3$@A-SiO_2 and $CsPbBr_3$@CC-SiO_2 (c), and $CsPbCl_3$@CA-SiO_2 and $CsPbI_3$@CA-SiO_2 (d).

By virtue of the facile synthetic process, we can also prepare $CsPbBr_3$@A-SiO_2 ($CsPbBr_3$ anchored on propylamine-capped silica) and $CsPbBr_3$@CC-SiO_2 ($CsPbBr_3$ anchored on octadecyl/carboxyl-capped silica) composites. TEM analysis indicated the corresponding morphology in Figure 4a and b. The anchored NCs distribute uniformly on SiO_2 particles, with average diameters between 6-14 nm. The crystallinity and elemental composition of $CsPbBr_3$@A-SiO_2 and $CsPbBr_3$@CC-SiO_2 were further confirmed by PXRD and XPS analysis (Figure S6). As expected, the $CsPbBr_3$@A-SiO_2 composite is brighter than $CsPbBr_3$@CC-SiO_2, and shows similar strong PL emission to $CsPbBr_3$@CA-SiO_2 (Figure 4c). Compared with $CsPbBr_3$@CA-SiO_2, the emission spectra of $CsPbBr_3$@A-SiO_2 and $CsPbBr_3$@CC-SiO_2 exhibits a slight red shift, with an emission maximum at 523 nm. A small shoulder at 495 nm can be detected for $CsPbBr_3$@CC-SiO_2, possibly attributable to the polar environment imposed by carboxylation. [29]

It is worthwhile to mention that halide perovskites feature flexible tunability of band gap via modulation of halide anion.[2-3] We prepared the $CsPbX_3$@CA-SiO_2 composites with various emission colors by using different lead halide precursors (from pure $PbCl_2$, and PbI_2 instead of $PbBr_2$) in the nanocrystal synthesis. Figure 4d shows the optical results of $CsPbCl_3$@CA-

SiO_2 and $CsPbI_3$@CA-SiO_2. Compared with the pure bromide sample of green emission (520 nm), $CsPbCl_3$@CA-SiO_2 and $CsPbI_3$@CA-SiO_2 composites show blue (427 nm) and red (650 nm) emissive fluorescence, yielding PLQYs of 28% and 67%, respectively (Figure 4d and Table S1).

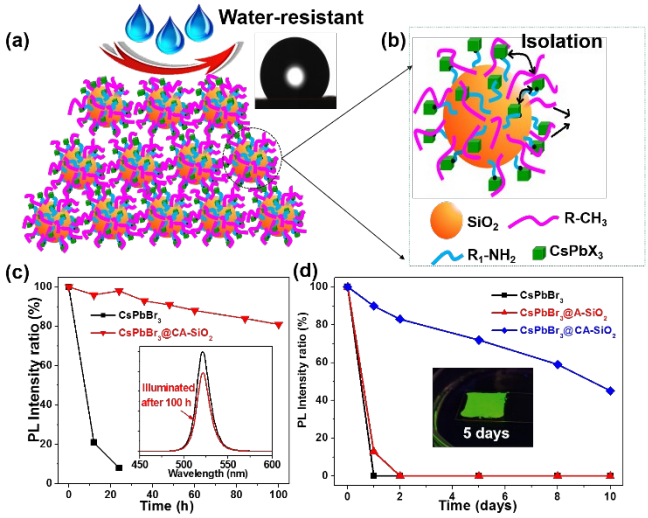

Figure 5. (a) Schematic illustration of the film surface of $CsPbBr_3$@CA-SiO_2 composites with dewetting property. Inserted in (a) is the photo showing the hydrophobicity of the WCAs. (b) Schematic illustration of $CsPbBr_3$@CA-SiO_2. (c) The relative PLQY plots against different UV irradiation times. Inset in (c) is the PL intensity before and after illuminated by UV light. (d) The relative PLQY plots of $CsPbBr_3$, $CsPbBr_3$@A-SiO_2 and $CsPbBr_3$@CA-SiO_2 films upon immersing in water over time. Inset in (d) is the photograph of the $CsPbBr_3$@CA-SiO_2 film taken under UV irradiation after immersion in water for 5 days.

The thus formed $CsPbBr_3$@CA-SiO_2 composite is expected to provide excellent dewetting properties and enhanced photostability. The photostability of $CsPbBr_3$@CA-SiO_2 composite was investigated by illuminating continuously under UV lamps (365 nm). The $CsPbBr_3$@CA-SiO_2 composite presents outstanding photostability, with no measurable PL intensity decrease after 24 hours of constant illumination. Even after 100 h, ~82% of the initial PL intensity was still maintained with no PL peak shift (Figure 5c). In contrast, the pure $CsPbBr_3$ film degraded from green to yellow upon illumination, and the PL intensity decreases dramatically over 24 h (Figure 5c). Clearly, although there are no discrete barrier layers, the NCs the $CsPbBr_3$@CA-SiO_2 composite are spatially isolated, which inhibits fusion, aggregation, and other proximity related degradation pathways.[28, 35, 37]

To measure the composite's water resistivity, we immersed solid films on glass slides into deionized water (Figure 5d). The relative PL of the $CsPbBr_3$@A-SiO_2 film decayed to 13% after 1 day and was fully quenched after 2 days. Neat perovskite films are completely quenched after 1 hour of water immersion. However, $CsPbBr_3$@CA-SiO_2 films present much higher stability, retaining 72% and 59% PLQY after immersing in water for 5 and 8 days (Figure 5d). Besides, the surface is hydrophobic, as suggested by a static water contact angle of 132° (insert in Figure 5a). The excellent dewetting property possibly results from the surface alkyl chains and micro/nano structural features (Figure 5a), surpassing previously reported encapsulated NCs.[32, 38-39] Photographs inserted in Figure 5d further confirm that the $CsPbBr_3$@CA-SiO_2 film remain highly fluorescent after immersing in water for 5 days. Compared with single SiO_2 particle-coated $CsPbX_3$ NCs that have exhibited enhanced stability,[24, 40] the *in-situ* growth method to anchor the $CsPbBr_3$ NCs on amino-ligand functionalized SiO_2 particles is superior in stabilizing the NCs by better spatial isolation of NCs and providing an excellent dewetting barrier to shield environmental agents.

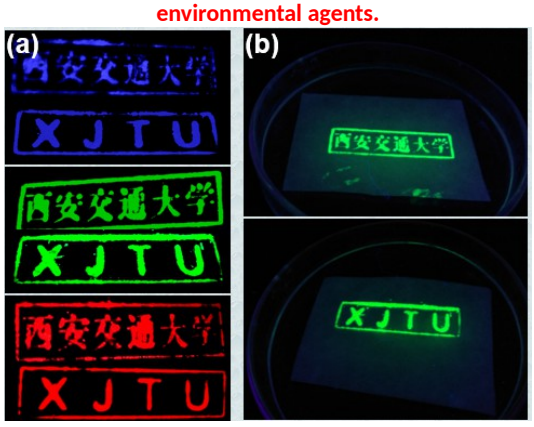

Figure 6. (a) Photograph of customized patterns containing $CsPbCl_3$@CA-SiO_2 (blue), $CsPbBr_3$@CA-SiO_2 (green) and $CsPbI_3$@CA-SiO_2 (red) under UV light. (b) Photograph of the patterns containing $CsPbBr_3$@CA-SiO_2 after immersion in water for 5h.

$CsPbBr_3$@CA-SiO_2 composite demonstrated excellent optical properties and high stability as the green fluorophore, which can be used in a proof of concept multicolor anti-counterfeiting security ink. As a demonstration, Figures 6a exhibited on a piece of filter paper under the 365 nm UV light by $CsPbCl_3$@CA-SiO_2, $CsPbBr_3$@CA-SiO_2 and $CsPbI_3$@CA-SiO_2 composite inks with hand carved seals, respectively. The ink is nearly colorless under room light but exhibits excellent uniformity and strong PL emission under UV light, emitting bright red, green and blue colors (Figure 6a). Besides, the high PL emission can be preserved even under immersion in water for 5 h, implying its excellent water stability (Figure 6b), which is superior than the other anti-counterfeiting security ink based on non-emissive Cs_4PbX_6 NCs.[41]

Besides, we also fabricated a down-converting white light emitting device (WLED).[25, 28, 40] Figure 7a illustrates the typical WLED device structure, in which YAG powder and $CsPbBr_3$@CA-SiO_2 are used as the red and green sources. Each layer is sequentially deposited onto a blue-emitting GaN chip. The electroluminescence (EL) spectrum of the prepared WLED device presents narrow green and broad red emission peaks at 525 nm and 660 nm, excited by the 460 nm GaN LED, attributed to the respective emission bands of $CsPbBr_3$@CA-SiO_2 and YAG phosphor.

Saturated and bright white emission can be clearly observed when the device is operated at a current of 20 mA (Figure 7b), featuring a CIE color coordinate (0.3225, 0.3468), very close to standard white emission (0.33, 0.33), indicating its

high color purity. The WLED device exhibits an acceptable luminous efficacy (LE) of 26.3 lm/W. The WLED device was highly stable at currents up to 140 mA (Figure 7c) and operating for 20 min at 20 mA (Figure S7), implying that the composite is a valuable light emitter even at high current densities. Therefore, the strong fluorescence, together with the improved stability verifies the great potential of the $CsPbBr_3$@CA-SiO_2 composite as a promising fluorophore for anticounterfeiting and wide-color gamut lighting and display devices.

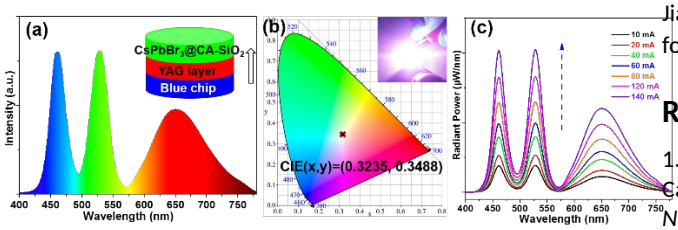

Figure 7. (a) EL emission spectra of the WLED. Inset in (a) is the schematics of the WLED, composed of GaN blue (460 nm) LED chips, $CsPbBr_3$@CA-SiO_2 films and YAG powder mixed with silicone resin as the blue, green and red light source. (b) CIE color coordinates of the fabricated devices with composite films. Inset in (b) is a photograph of a working device with an applied current of 20 mA. (c) EL spectra of fabricated WLED under various operation currents.

Conclusion

In summary, we report a facile synthesis of highly luminescent and stable $CsPbX_3$@CA-SiO_2 nanocomposites. The silica NPs capped with octadecyl and propylamine groups (appr. 120 nm) were employed as templates for perovskite NCs growth, yielding monodisperse NCs (~6 nm) anchored onto SiO_2 NPs. The resulting composites exhibit a high photoluminescence quantum yield (76%), tunable anion-dependent emission wavelength, enhanced photostability and remarkable water stability compared to previously reported encapsulated NCs. The $CsPbX_3$@CA-SiO_2 composite can be used as an anti-counterfeit ink and a fluorophore for WLED, indicating their promising potentials in solid-state optoelectronics. We believe this work will open the door for future research into multifunctional perovskite-based composites for real-world optoelectronic applications.

Conflicts of interest

The authors declare no competing financial interest.

Acknowledgements

This work was supported by the National Natural Science Foundation of China (NSFC Grants 51802254, 51873173), the China Postdoctoral Science Foundation Funded Project (2017M623149), the Fundamental Research Funds for the Central Universities (xjj2018053) and Shaanxi province Youth Foundation (2018JQ5011). Part of the work was also supported by the U.S. Department of Energy, Office of Science, Office of Basic Energy Sciences, Materials Sciences and Engineering Division, under Contract No. DE-AC02-05-CH11231 within the Inorganic/Organic Nanocomposites Program (KC3104) (MJ and YL). Work at the Molecular Foundry was supported by the Office of Science, Office of Basic Energy Sciences, of the U.S. Department of Energy under Contract No. DE-AC02-05CH11231. The authors wish to express their gratitude to the MOE Key Laboratory for Nonequilibrium Condensed Matter and Quantum Engineering of Xi'an Jiaotong University. The authors also thank Jiao Li at Instrument Analysis Center of Xi'an Jiaotong University for their assistance with TEM analysis.

References

1. L. Protesescu, S. Yakunin, M. I. Bodnarchuk, F. Krieg, R. Caputo, C. H. Hendon, R. X. Yang, A. Walsh and M. V. Kovalenko, *Nano Lett.*, 2015, **15**, 3692-3696.
2. G. Nedelcu, L. Protesescu, S. Yakunin, M. I. Bodnarchuk, M. J. Grotevent and M. V. Kovalenko, *Nano Lett.*, 2015, **15**, 5635-5640.
3. Q. A. Akkerman, V. D'Innocenzo, S. Accornero, A. Scarpellini, A. Petrozza, M. Prato and L. Manna, *J. Am. Chem. Soc.*, 2015, **137**, 10276-10281.
4. A. Swarnkar, R. Chulliyil, V. K. Ravi, M. Irfanullah, A. Chowdhury and A. Nag, *Angew. Chem. Int. Ed. Engl.*, *2015*, **54**, 15424-15428.
5. Kovalenko V. Maksym, P. L. and Bodnarchuk M. I., *Science*, 2017, **358**, 745-750.
6. S. A. Veldhuis, P. P. Boix, N. Yantara, M. Li, T. C. Sum, N. Mathews and S. G. Mhaisalkar, *Adv. Mater.*, 2016, **28**, 6804-6834.
7. S. Yakunin, L. Protesescu, F. Krieg, M. I. Bodnarchuk, G. Nedelcu, M. Humer, G. D. Luca, M. Fiebig, W. Heiss and M. V. Kovalenko, *Nat. Commun.*, 2015, **6**, 8056-8063.
8. Y. H. Kim, S. Jo, S. H. Lee and W. T., *Small Methods*, 2018, 1800093-1800113.
9. H. Cho, Y. H. Kim, C. Wolf, H. D. Lee and T. W. Lee, *Adv. Mater.*, 2018, **30**, 1704587-1704611.
10. T. Leijtens, G. E. Eperon, N. K. Noel, S. N. Habisreutinger, A. Petrozza and H. J. Snaith, *Adv. Energy Mater.*, 2015, **5**, 1500963-1500986.
11. J. De Roo, M. Ibanez, P. Geiregat, G. Nedelcu, W. Walravens, J. Maes, J. C. Martins, I. Van Driessche, M. V. Kovalenko and Z. Hens, *ACS Nano*, 2016, **10**, 2071-2081.
12. D. Parobek, Y. Dong, T. Qiao, D. Rossi and D. H. Son, *J. Am. Chem. Soc.*, 2017, **139**, 4358-4361.
13. Y. Kim, E. Yassitepe, O. Voznyy, R. Comin, G. Walters, X. Gong, P. Kanjanaboos, A. F. Nogueira and E. H. Sargent, *ACS Appl. Mater. Interfaces*, 2015, **7**, 25007-25013.
14. S. Huang, Z. Li, B. Wang, N. Zhu, C. Zhang, L. Kong, Q. Zhang, A. Shan and L. Li, *ACS Appl. Mater. Interfaces*, 2017, **9**, 7249-7258.
15. Z. Dang, J. Shamsi, F. Palazon, M. Imran, Q. A. Akkerman, S. Park, G. Bertoni, M. Prato, R. Brescia and L. Manna, *ACS Nano*, 2017, **11**, 2124-2132.
16. J. Pan, L. N. Quan, Y. Zhao, W. Peng, B. Murali, S. P. Sarmah, M. Yuan, L. Sinatra, N. M. Alyami, J. Liu, E. Yassitepe, Z. Yang, O. Voznyy, R. Comin, M. N. Hedhili, O. F. Mohammed, Z. H. Lu, D. H. Kim, E. H. Sargent and O. M. Bakr, *Adv. Mater.*, 2016, **28**, 8718-8725.

17. B. Luo, Y. C. Pu, S. A. Lindley, Y. Yang, L. Lu, Y. Li, X. Li and J. Z. Zhang, *Angew. Chem. Int. Ed. Engl.*, 2016, **55**, 8864-8868.
18. A. Z. Pan, J. L. Wang, M. J. Jurow , M. J. Jia, Y. S. Wu, Y. Liu, Y. F. Zhang, L. He and Y. Liu, *Chem. Mater.*, 2018, **30**, 2771-2780.
19. H. Huang, B. Chen, Z. Wang, T. F. Hung, A. S. Susha, H. Zhong and A. L. Rogach, *Chem. Sci.*, 2016, **7**, 5699-5703.
20. M. Imran, V. Caligiuri, M. Wang, L. Goldoni, M. Prato, R. Krahne, L. De Trizio and L. Manna, *J. Am. Chem. Soc.*, 2018, **140**, 2656-2664.
21. S. Zou, Y. Liu, J. Li, C. Liu, R. Feng, F. Jiang, Y. Li, J. Song, H. Zeng, M. Hong and X. Chen, *J. Am. Chem. Soc.*, 2017, **139**, 11443-11450.
22. Q. A. Akkerman, D. Meggiolaro, Z. Dang, F. De Angelis and L. Manna, *ACS Energy Lett.*, 2017, **2**, 2183-2186.
23. J.-Y. Sun, F. T. Rabouw, X.-F. Yang, X.-Y. Huang, X.-P. Jing, S. Ye and Q.-Y. Zhang, *Adv. Funct. Mater.*, 2017, **27**, 1704371-1704379.
24. Q. Zhong, M. Cao, H. Hu, D. Yang, M. Chen, P. Li, L. Wu and Q. Zhang, *ACS Nano*, 2018, **12**, 8579-8587.
25. C. Sun, Y. Zhang, C. Ruan, C. Yin, X. Wang, Y. Wang and W. W. Yu, *Adv. Mater.*, 2016**, 28**, 10088-10094.
26. C. Zhang, B. Wang, W. Li, S. Huang, L. Kong, Z. Li and L. Li, *Nat. Commun.*, 2017, **8**, 1138.
27. S. N. Raja, Y. Bekenstein, M. A. Koc, S. Fischer, D. Zhang, L. Lin, R. O. Ritchie, P. Yang and A. P. Alivisatos, *ACS Appl. Mater. Interfaces*, 2016, **8**, 35523-35533.
28. A. Pan, J. Wang, M. J. Jurow, M. Jia, Y. Liu, Y. Wu, Y. Zhang, L. He and Y. Liu, *Chem. Mater.*, 2018, **30**, 2771-2780.
29. A. Pan, M. J. Jurow, F. Qiu, J. Yang, B. Ren, J. J. Urban, L. He and Y. Liu, *Nano Lett.*, 2017, **17**, 6759-6765.
30. Q. A. Akkerman, G. Raino, M. V. Kovalenko and L. Manna, *Nat. Mater.*, 2018, **17**, 394-405.
31. X. Li, Y. Wang, H. Sun and H. Zeng, *Adv. Mater.*, 2017, **29**, 1701185-1701194.
32. S. Hou, Y. Guo, Y. Tang and Q. Quan, *ACS Appl. Mater. Interfaces*, 2017, **9**, 18417-18422.
33. S. Werner, F. A. and B. Ernst, *J. Colloid Interf. Sci.*, 1968, **26**, 62-69.
34. D. Chen, S. Yuan, X. Chen, J. Li, Q. Mao, X. Li and J. Zhong, *J. Mater. Chem. C*, 2018, **6**, 6832-6839.
35. S. Yuan, D. Chen, X. Li, J. Zhong and X. Xu, *ACS Appl. Mater. Interfaces*, 2018, **10**, 18918-18926.
36. S. Lou, T. Xuan, C. Yu, M. Cao, C. Xia, J. Wang and H. Li, *J. Mater. Chem. C*, 2017, **5**, 7431-7435.
37. A. Loiudice, S. Saris, E. Oveisi, D. T. L. Alexander and R. Buonsanti, *Angew. Chem. Int. Ed. Engl.*, 2017, **56**, 10696-10701.
38. T. Xuan, X. Yang, S. Lou, J. Huang, Y. Liu, J. Yu, H. Li, K. L. Wong, C. Wang and J. Wang, *Nanoscale*, 2017, **9**, 15286-15290.
39. J. Hai, H. Li, Y. Zhao, F. Chen, Y. Peng and B. Wang, *Chem. Commun.*, 2017, **53**, 5400-5403.
40. H. Hu, L. Wu, Y. Tan, Q. Zhong, M. Chen, Y. Qiu, D. Yang, B. Sun, Q. Zhang and Y. Yin, *J. Am. Chem. Soc.*, 2018, **140**, 406-412.
41. X. Yu, L. Wu, H. Hu, M. Chen, Y. Tan, D. Yang, Q. Pan, Q. Zhong, T. Supasai and Q. Zhang, *Langmuir*, 2018, **34**, 10363-10370.42. T. Guner and M. M. Demir, *Phys. Status Solidi A*, 2018, **215**, 1800120-1800131.